ELECTROMAGNETIC SCATTERING FROM A RESISTIVE HALF PLANE ON A DIELECTRIC INTERFACE

John L. VOLAKIS and Jeffrey D. COLLINS

Radiation Laboratory, Electrical Engineering and Computer Science, The University of Michigan, Ann Arbor, MI 48109-2122, U.S.A.

The dual integral equation approach is employed to determine the diffracted field from a resistive half plane on a dielectric interface. A solution is obtained by introducing two Wiener–Hopf split functions, one being inherent to the dielectric interface problem and the other characteristic to the presence of the resistive sheet. Uniform asymptotic expressions for the E- and H-polarizations are given (with the exception of the branch cut contribution), and numerical computations are included for the far-zone and near-zone fields. Also, a convenient integral expression is given in the Appendix for the evaluation of the split functions.

1. Introduction

The problem of interest is that of plane wave diffraction by a resistive half plane on a dielectric interface, shown in Fig. 1. Such a geometry may represent a number of physical situations depending on the chosen resistivity, R, of the resistive half sheet. For example, it may represent a small dielectric step discontinuity as shown in Fig. 2 [1, 2] or the presence of a thin conducting half sheet of finite conductivity at the surface of the interface.

The solution of the stated diffraction problem is obtained herein via application of the angular spectrum method (ASM) set forth by Booker and Clemmow [3, 4]. This method is often referred to as the dual integral equation approach and involves the representation of the scattered field by an angular spectrum of plane waves emanating from the edge of the half sheet. It is in all respects equivalent to the Wiener–Hopf technique, but requires fewer steps since in the ASM all explicit Fourier transformations are avoided.
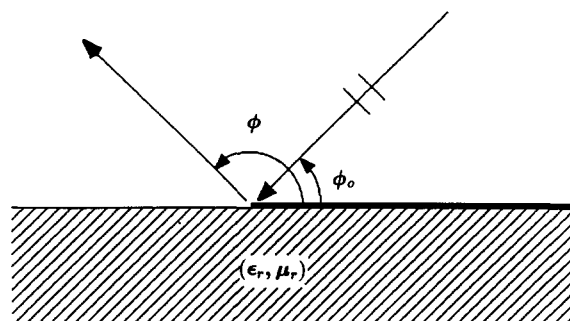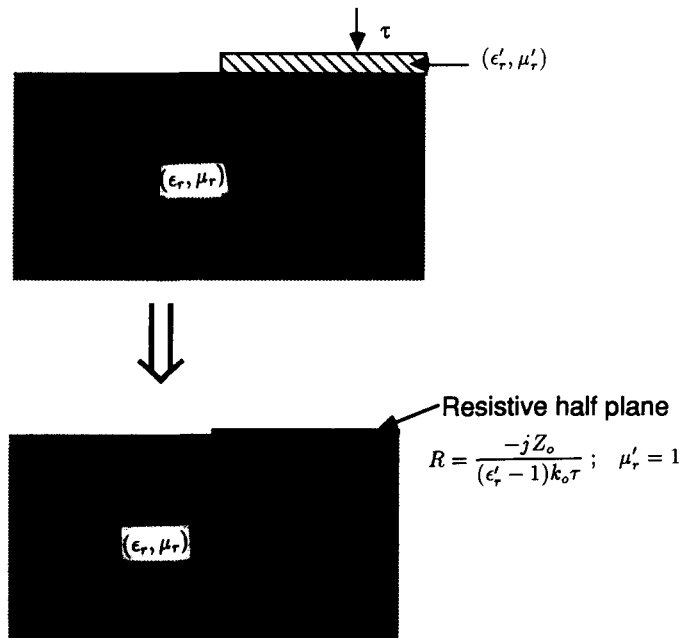

Fig. 1. Geometry of the problem.

Fig. 2. The simulation of a dielectric step discontinuity using a resistive sheet on a dielectric interface.

Thus, as in the Wiener–Hopf technique, the usual factorizations must also be done, an often impossible task to accomplish analytically.

The ASM was initially applied by Clemmow [4] to the problem of diffraction by an isolated and a pair of perfectly conducting half planes. More recently, the method was employed for the treatment of the diffraction by thick perfectly conducting [5] and impedance [6] half planes. A solution of the diffraction by a thick metal-dielectric junction has also been obtained by Ricoy and Volakis [7] using the ASM. Returning to the problem at hand, Coblin and Pearson [8] obtained an E-polarization solution for the special case, of $R = 0$ using the Wiener–Hopf technique. Clemmow [9] also attempted a solution to the problem but did not present an expression for the resulting split function for which a convenient integral expression is given in [8]. This, and an additional new split function will be encountered in the more general case of $R \neq 0$ treated here.

Below, we first consider the H-polarization case, and a similar analysis follows for E-polarization. In either case uniform asymptotic expressions for the total field are presented. These account for the geometrical optics and surface wave poles and were used to compute the included diffraction patterns. As expected, the computation required a numerical evaluation of the resulting split functions, and a convenient general integral expression (than those available) for accomplishing this is given in the Appendix.

2. H-polarization

2.1. Analysis

Consider the plane wave

$$H^i = \hat{z}\, e^{jk\rho \cos(\phi - \phi_0)} \tag{1}$$

incident at an angle ϕ_0 upon the geometry of interest shown in Fig. 1. The resistive sheet comprising this

geometry has resistivity R and occupies the half plane $x > 0$, $y = 0$. In addition, the dielectric is assumed to be linear, isotropic and homogeneous with relative permeability and permittivity μ_r and ε_r, respectively. In (1), (ρ, ϕ) are the usual cylindrical coordinates, k is the free space propagation factor and an $e^{j\omega t}$ time dependence has been assumed and suppressed.

As usual, the dielectric interface alone causes a reflected and a transmitted field. The presence of the resistive half plane, however, will also give rise to an additional scattered field that can be represented by [4, 9]

$$H_z^s = \int_C P^h(\cos \alpha) \, e^{-jk\rho \, \cos(\phi - \alpha)} \, d\alpha \tag{2}$$

in the region $y > 0$ and by

$$H_z^{st} = - \int_C P^h(\cos \alpha) \sqrt{\frac{\varepsilon_r}{\mu_r} \frac{\sin \alpha}{\sin \alpha_t}} \, e^{-jk_t\rho \, \cos(\phi + \alpha_t)} \, d\alpha \tag{3}$$

in the region $y < 0$, where $k_t = \kappa k$. The integration path is indicated in Fig. 3b, and to ensure continuity of the tangential fields at the interface, we must set $k \cos \alpha = k_t \cos \alpha_t$. Lastly, $P^h(\cos \alpha)$ is an unknown function related to the angular spectrum of the current flowing on the resistive half plane. Its evaluation is the underlying task in this section.

In proceeding with the solution of $P^h(\cos \alpha)$, it is necessary to employ the appropriate boundary conditions. These are

A. Continuity of H_z over $x < 0$ and $y = 0$,
B. $E_x = R[H_z(y = 0^+) - H_z(y = 0^-)]$ over $x > 0$ and $y = 0$

where H_z and E_x represent total fields and we can write the H_z component as

$$H_z = \begin{cases} H_z^i + H_z^r + H_z^s, & y > 0, \\ H_z^t + H_z^{st}, y < 0 \end{cases} \tag{4}$$

where H_z^t and H_z^r are the transmitted and reflected fields, respectively, in the absence of the resistive half plane. Since $H_z^i + H_z^r = H_z^t$ at $y = 0$, the application of condition A yields

$$\int_{-\infty}^{\infty} \left(\frac{\sqrt{\kappa^2 - \lambda^2} + \varepsilon_r \sqrt{1 - \lambda^2}}{\sqrt{\kappa^2 - \lambda^2} \sqrt{1 - \lambda^2}} \right) P^h(\lambda) \, e^{-jkx\lambda} \, d\lambda = 0, \quad y = 0, \, x < 0 \tag{5}$$

in which $\lambda = \cos \alpha$, $\kappa^2 = \varepsilon_r \mu_r$ and Z_0 is the intrinsic impedance of free space. Similarly, application of condition B yields

$$\int_{-\infty}^{\infty} P^h(\cos \alpha) \left[\frac{R}{Z_0} \left(\frac{1}{\sqrt{1 - \lambda^2}} + \frac{\varepsilon_r}{\sqrt{\kappa^2 - \lambda^2}} \right) + 1 \right] e^{-jkx\lambda} \, d\lambda = \frac{2\sqrt{1 - \lambda_0^2} \sqrt{\kappa^2 - \lambda_0^2}}{\varepsilon_r \sqrt{1 - \lambda_0^2} + \sqrt{\kappa^2 - \lambda_0^2}} \, e^{jkx\lambda_0}, \quad y = 0, \, x > 0 \tag{6}$$

with $\lambda_0 = \cos \phi_0$. The integration path for (5) and (6) is given in Fig. 3a.

Equations (5) and (6) can be decoupled by invoking Cauchy's theorem. From (5) we find that

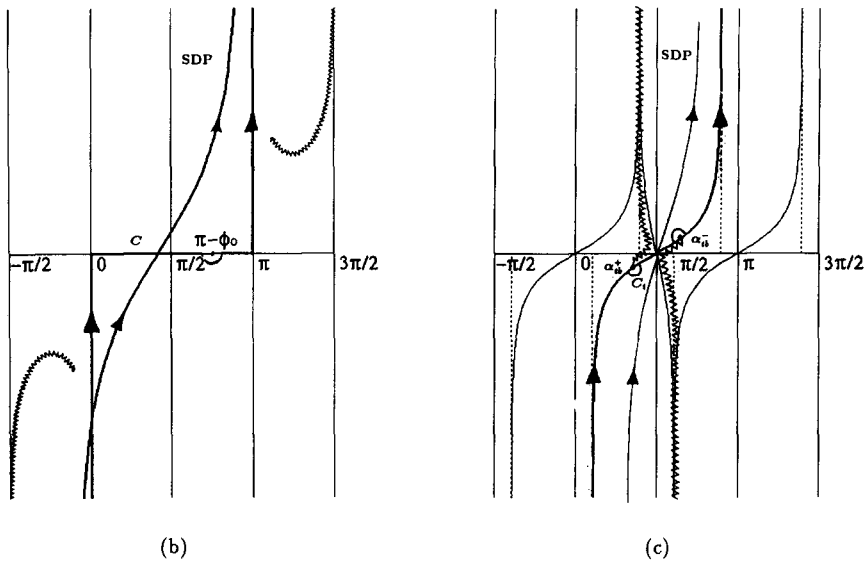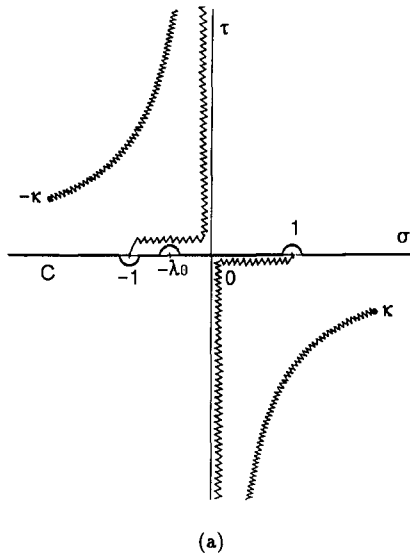$$P^h(\lambda) = \frac{\sqrt{1 + \lambda} \sqrt{\kappa + \lambda}}{G_-(\lambda)} U(\lambda) \tag{7}$$

Fig. 3. Integration contours in the (a) λ-plane, (b) α-plane, and (c) α_t-plane.

where $U(\lambda)$ is some unknown function free of zeros, poles and branch points (i.e., regular) in the upper half of the λ-plane. In addition, $G_-(\lambda)$ is regular in the lower half of the λ-plane, satifying the relation

$$G(\lambda) = G_-(\lambda)\, G_+(\lambda) = \varepsilon_r\sqrt{1-\lambda^2} + \sqrt{\kappa^2 - \lambda^2} \tag{8}$$

with $G_-(\lambda) = G_+(-\lambda)$. Similarly, (6) implies

$$P^h(\lambda)\left[\frac{R}{Z_0}\left(\frac{\varepsilon_r\sqrt{1-\lambda^2}+\sqrt{\kappa^2-\lambda^2}}{\sqrt{1-\lambda^2}\,\sqrt{\kappa^2-\lambda^2}}\right)+1\right] = -\frac{1}{j\pi}\frac{\sqrt{1-\lambda_0^2}\,\sqrt{\kappa^2-\lambda_0^2}}{\varepsilon_r\sqrt{1-\lambda_0^2}+\sqrt{\kappa^2-\lambda_0^2}}\frac{1}{\lambda+\lambda_0}\frac{L(\lambda)}{L(-\lambda_0)} \tag{9}$$

where $L(\lambda)$ is again an unknown function regular in the lower half of the λ-plane. To solve for the functions $U(\lambda)$ and $L(\lambda)$ in (7) and (9) we must first introduce the function

$$J(\lambda) = J_+(\lambda) \, J_-(\lambda) = \frac{R}{Z_0} \left(\frac{\varepsilon_r \sqrt{1 - \lambda^2} + \sqrt{\kappa^2 - \lambda^2}}{\sqrt{1 - \lambda^2} \sqrt{\kappa^2 - \lambda^2}} \right) + 1 \tag{10}$$

with $J_-(\lambda) = J_+(-\lambda)$ being regular on the lower half of the λ-plane. Since $U(\lambda)$ and $L(\lambda)$ are associated with different regions of regularity, by substituting (7) into (9) we obtain

$$L(\lambda) = \frac{\sqrt{1 + \lambda} \, \sqrt{\kappa + \lambda}}{G_-(\lambda)} \, J_-(\lambda), \tag{11}$$

implying

$$P^{\mathrm{h}}(\cos \alpha) = \frac{\mathrm{j}}{\pi} \frac{\sqrt{1 + \cos \phi_0} \, \sqrt{\kappa + \cos \phi_0} \, \sqrt{1 + \cos \alpha} \, \sqrt{\kappa + \cos \alpha}}{G_-(\cos \alpha) \, G_-(\cos \phi_0) \, J_+(\cos \alpha) \, J_+(\cos \phi_0)} \frac{1}{\cos \alpha + \cos \phi_0}. \tag{12}$$

In (12), the split function $G_-(\lambda)$ and $J_+(\lambda)$ must be evaluated numerically, and a convenient integral expression for either of them is given in the Appendix. $G_-(\lambda)$ has already been encountered in [8] where an equally convenient, but different, integral expression was given there for its evaluation. The function $J_+(\lambda)$ is characteristic to this problem and reduces to unity when $R = 0$ or to the usual split function encountered in [2], [10] in the case of diffraction by an isolated impedance or resistive half plane.

2.2. Uniform asymptotic evaluation

The integral expression (2) with $P^{\mathrm{h}}(\cos \alpha)$ as given in (12) is amenable to an asymptotic evaluation via the method of steepest descents. A similar evaluation can also be pursued for (3) and to do so, it is useful to invoke the relation $\cos \alpha = \kappa \cos \alpha_t$ to rewrite H_z^{st} as

$$H_z^{\mathrm{st}} = -\varepsilon_r \int_{C_t} P^{\mathrm{h}}(\kappa \cos \alpha_t) \, \mathrm{e}^{-\mathrm{j} k_t \rho \cos(\phi + \alpha_t)} \, \mathrm{d}\alpha_t, \quad y < 0 \tag{13}$$

where

$$P^{\mathrm{h}}(\kappa \cos \alpha_t) = \frac{\mathrm{j}}{\pi} \frac{\sqrt{1 + \cos \phi_0} \, \sqrt{\kappa + \cos \phi_0} \, \sqrt{1 + \kappa \cos \alpha_t} \, \sqrt{\kappa + \kappa \cos \alpha_t}}{G_-(\kappa \cos \alpha_t) \, G_-(\cos \phi_0) \, J_+(\kappa \cos \alpha_t) \, J_+(\cos \phi_0)} \frac{1}{\kappa \cos \alpha_t + \cos \phi_0} \tag{14}$$

and C_t is illustrated in Fig. 3c.

The pertinent saddle points for a steepest descent path (SDP) evaluation of (2) and (3) are

$$\alpha_s = \phi, \qquad y > 0, \tag{15}$$

$$\alpha_{ts} = 2\pi - \phi, \quad y < 0, \tag{16}$$

and to derive a uniform expression, it is necessary to consider any poles and branch cuts encountered in the deformation of the original path of integration to the SDP. We find that the integrand is associated with the geometrical optics poles located at

$$\alpha_{\mathrm{go}}^{\pm} = \pi \pm \phi_0, \qquad y > 0, \tag{17}$$

$$\alpha_{\mathrm{tgo}}^{\pm} = \pm \cos^{-1}\left(\frac{-\cos \phi_0}{\kappa} \right), \quad y < 0. \tag{18}$$

In addition, a surface wave pole may exist in accordance with the relations

$$J_+(\cos \alpha_{sw}) = 0, \qquad y > 0, \tag{19}$$

$$J_+(\kappa \cos \alpha_{tsw}) = 0, \quad y < 0. \tag{20}$$

$P^h(\kappa \cos \alpha_t)$ also exhibits branch point singularities at

$$\alpha_{tb}^\pm = \cos^{-1}\left(\pm\frac{1}{\kappa}\right), \tag{21}$$

implicit in the functions $G_-(\kappa \cos \alpha_t)$ and $J_+(\kappa \cos \alpha_t)$ containing the square root functions $\sqrt{1 + \kappa \cos \alpha_t}$ and $\sqrt{1 - \kappa \cos \alpha_t}$, respectively.

Excluding the branch cut contribution, we may employ the procedure given in [11] to obtain

$$
\begin{aligned}
H_z^s \sim{} & \sqrt{\frac{2\pi}{k\rho}}\, P^h(\cos \phi)\, e^{-jk\rho}\, e^{j\pi/4} \\
&+ \frac{1}{2}\sqrt{\frac{2\pi}{k\rho}}\, \frac{t_1^h(\alpha_{go}^-, \phi_0)}{\sin \alpha_{go}^-}\sec\left(\frac{\phi - \alpha_{go}^- + \pi}{2}\right)\left\{1 - F_{kp}\left[2k\rho\,\cos^2\left(\frac{\phi - \alpha_{go}^- + \pi}{2}\right)\right]\right\} e^{-jk\rho}\, e^{j\pi/4} \\
&+ \frac{1}{2}\sqrt{\frac{2\pi}{k\rho}}\, \frac{t_1^h(\alpha_{go}^+, \phi_0)}{\sin \alpha_{go}^+}\sec\left(\frac{\phi - \alpha_{go}^+ - \pi}{2}\right)\left\{1 - F_{kp}\left[2k\rho\,\cos^2\left(\frac{\phi - \alpha_{go}^+ - \pi}{2}\right)\right]\right\} e^{-jk\rho}\, e^{j\pi/4} \\
&- \frac{1}{2}\sqrt{\frac{2\pi}{k\rho}}\, \frac{t_2^h(\alpha_{sw}, \phi_0)}{J'(\cos \alpha_{sw})}\sec\left(\frac{\phi - \alpha_{sw} + \pi}{2}\right)\left\{1 - F_{kp}\left[2k\rho\,\cos^2\left(\frac{\phi - \alpha_{sw} + \pi}{2}\right)\right]\right\} e^{-jk\rho}\, e^{j\pi/4}
\end{aligned}
\tag{22}
$$

for $y > 0$ and

$$
\begin{aligned}
H_z^{st} \sim{} & -\varepsilon_r\Bigg\{ \sqrt{\frac{2\pi}{\kappa k\rho}}\, P^h(\kappa \cos \phi)\, e^{-j\kappa k\rho}\, e^{j\pi/4} \\
&+ \frac{1}{2}\sqrt{\frac{2\pi}{\kappa k\rho}}\, \frac{t_{1t}^h(\alpha_{tgo}^-, \phi_0)}{\kappa \sin \alpha_{tgo}^-}\sec\left(\frac{\phi + \alpha_{tgo}^- - \pi}{2}\right)\left\{1 - F_{kp}\left[2\kappa k\rho\,\cos^2\left(\frac{\phi + \alpha_{tgo}^- - \pi}{2}\right)\right]\right\} e^{-j\kappa k\rho}\, e^{j\pi/4} \\
&+ \frac{1}{2}\sqrt{\frac{2\pi}{\kappa k\rho}}\, \frac{t_{1t}^h(\alpha_{tgo}^+, \phi_0)}{\kappa \sin \alpha_{tgo}^+}\sec\left(\frac{\phi + \alpha_{tgo}^+ + \pi}{2}\right)\left\{1 - F_{kp}\left[2\kappa k\rho\,\cos^2\left(\frac{\phi + \alpha_{tgo}^+ + \pi}{2}\right)\right]\right\} e^{-j\kappa k\rho}\, e^{j\pi/4} \\
&- \frac{1}{2}\sqrt{\frac{2\pi}{\kappa k\rho}}\, \frac{t_{2t}^h(\alpha_{tsw}, \phi_0)}{J'(\cos \alpha_{tsw})}\sec\left(\frac{\phi + \alpha_{tsw} + \pi}{2}\right)\left\{1 - F_{kp}\left[2\kappa k\rho\,\cos^2\left(\frac{\phi + \alpha_{tsw} + \pi}{2}\right)\right]\right\} e^{-j\kappa k\rho}\, e^{j\pi/4}\Bigg\}
\end{aligned}
\tag{23}
$$

for $y < 0$. In the above

$$t_1^h(\alpha, \phi_0) = P^h(\cos \alpha)(\cos \phi_0 + \cos \alpha), \tag{24}$$

$$t_{1t}^h(\alpha_t, \phi_0) = P^h(\kappa \cos \alpha_t)(\cos \phi_0 + \kappa \cos \alpha_t), \tag{25}$$

$$t_2^h(\alpha, \phi_0) = P^h(\cos \alpha)\,\frac{J_+(-\cos \alpha)\, J_+(\cos \alpha)}{J(\cos \alpha)}, \tag{26}$$

$$t_{2t}^h(\alpha_t, \phi_0) = P^h(\kappa \cos \alpha_t)\,\frac{J_+(-\kappa \cos \alpha_t)\, J_+(\kappa \cos \alpha_t)}{J(\kappa \cos \alpha_t)}. \tag{27}$$

Also, $J'(\cos \alpha_{sw})$ and $J'(\kappa \cos \alpha_{tsw})$ denote the derivatives of J with respect to α and α_t, respectively, evaluated at the location of the surface wave pole. The $F_{kp}(z^2)$ function is the Kouyoumjian–Pathak transition function [2, 12] defined as

$$F_{kp}(z^2) = \pm 2jz\, e^{jz^2} \int_{\pm z}^{\infty} e^{-jt^2}\, dt \tag{28}$$

where the sign is chosen such that total field continuity is maintained at the geometrical optics and surface wave field boundaries. Here, choosing the lower sign satisfies this condition. In passing, we note that in (22) and (23) the first term is the usual nonuniform diffracted field, while the remaining ones are the geometrical optics and surface wave contributions. Consistent with the definition in [12], the non-uniform diffraction coefficient is given by

$$D^h(\phi, \phi_0) = \sqrt{\frac{2\pi}{k}}\, P^h(\kappa \cos \phi)\, e^{j\pi/4}, \qquad y > 0, \tag{29}$$

$$D_t^h(\phi, \phi_0) = -\varepsilon_r \sqrt{\frac{2\pi}{\kappa k}}\, P^h(\kappa \cos \phi)\, e^{j\pi/4}, \qquad y < 0. \tag{30}$$

To perform a uniform evaluation of the branch cut contribution, it is first suggestive to replace $G_-(\lambda)$ by $G(\lambda)/G_+(\lambda)$ and $J_+(\lambda)$ by $J(\lambda)/J_-(\lambda)$. Since both $G_-(\lambda)$ and $J_+(\lambda)$ are evaluated numerically, the introduction of $G(\lambda)$ and $J(\lambda)$ is required to allow a subsequent analytical treatment of the square roots associated with the branch cuts that are likely to cross the SDP. Of these, the one associated with $G(\lambda)$ is the most dominant among the two, and its contribution yields the lateral wave that is inherent to the interface problem. Further, to employ available techniques for the uniform evaluation of the branch cut contribution, it is necessary to regularize the denominator and to bring the square root to the numerator.
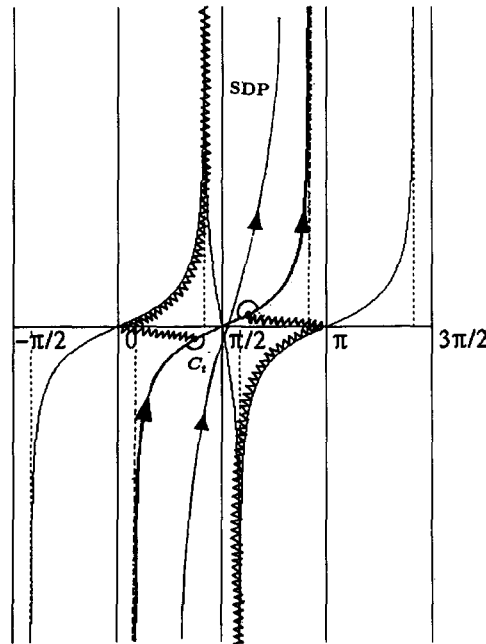

Fig. 4. The modified branch cut in the α_t-plane.

This procedure yields a pair of integrand terms, one of which is regular in the region of interest and the other contains the root exhibiting the branch cut singularity. The first would thus require a non-uniform evaluation, whereas the second must be evaluated uniformly, resulting in the introduction of parabolic cylinder functions of fractional order.

Although the above appears to be a natural approach, to ensure the cancellation of a ficticious pole introduced in the process of bringing the square root to the numerator, it is necessary to maintain the same order in $k\rho$ for both evaluations. This demands the inclusion of high order terms in the non-uniform evaluation, a rather tedious task, requiring knowledge of higher order integrand derivatives [13]. Further, our attempt to ensure the pole cancellation via heuristic modifications was not successful because of the rapidly varying nature of the result near the lateral wave boundary. Therefore, since the lateral wave contribution is relatively small and progressively diminishes as $k\rho$ increases, it was not included in our uniform field evaluation. Instead, to avoid complications with the expected crossing of the branch cuts in the region $\phi > \pi$, those associated with the branch points at $\lambda = \pm 1$ were deformed from their conventional path as illustrated in Fig. 4.

3. *E*-polarization

Through parallel analysis, one can arrive at a solution for *E*-polarization incidence. In this case, the incident field is

$$E^i = \hat{z}\, e^{jk\rho\,\cos(\phi-\phi_0)} \tag{31}$$

and the required boundary conditions are

A. Continuity of H_x over $x < 0$ and $y = 0$,

B. $E_z = -R[H_x(y = 0^+) - H_x(y = 0^-)]$ over $x > 0$ and $y = 0$,

C. Continuity of E_z over $y = 0$

where

$$E_z = \begin{cases} E_z^i + E_z^r + E_z^s, & y > 0, \\ E_z^t + E_z^{st} & y < 0 \end{cases} \tag{32}$$

is the total field. As before, E_z^r and E_z^t correspond to the fields reflected from and transmitted into the interface, respectively, in the absence of the resistive half plane. In addition, E_z^s and E_z^{st} are the scattered fields caused by the presence of the resistive half plane and can be expressed as

$$E_z^s = \int_C P^e(\cos\alpha)\, e^{-jk\rho\,\cos(\phi-\alpha)}\, d\alpha, \qquad y > 0, \tag{33}$$

$$E_z^{st} = \kappa \int_{C_t} Q(\kappa\cos\alpha_t)\, e^{-jk_t\rho\,\cos(\phi+\alpha_t)}\, d\alpha_t, \qquad y < 0 \tag{34}$$

where the paths C and C_t are as stated previously. Through application of the boundary conditions, it is then found that

$$P^e(\cos\alpha) = \frac{1}{j\pi} \frac{\mu_r\sin\phi_0\sin\alpha}{N_+(\cos\alpha)\,N_+(\cos\phi_0)\,M_-(\cos\alpha)\,M_-(\cos\phi_0)} \frac{1}{\cos\phi_0+\cos\alpha} \tag{35}$$

and

$$Q(\kappa \cos \alpha_t) = \frac{1}{j\pi} \frac{\mu_r \sin \phi_0 \sin \alpha_t}{N_+(\kappa \cos \alpha_t) N_+(\cos \phi_0) M_-(\kappa \cos \alpha_t) M_-(\cos \phi_0)} \frac{1}{\cos \phi_0 + \kappa \cos \alpha_t} \qquad (36)$$

in which $N_+(\lambda)$ and $M_-(\lambda)$ are the pertinent Wiener–Hopf split functions satisfying the relations

$$M(\lambda) = M_+(\lambda) M_-(\lambda) = \mu_r\sqrt{1-\lambda^2} + \sqrt{\kappa^2 - \lambda^2}, \qquad (37)$$

$$N(\lambda) = N_+(\lambda) N_-(\lambda) = 1 + \frac{R}{\mu_r Z_0}(\mu_r\sqrt{1-\lambda^2} + \sqrt{\kappa^2 - \lambda^2}). \qquad (38)$$

Their evaluation must again be performed using the integral expression in the Appendix.

In performing a uniform asymptotic evaluation of (33) and (34) we find that the location of the relevant saddle points, geometrical optics poles and branch cuts remain the same as for *H*-polarization. The only difference is the specific location of the surface wave pole, α_{sw}, satisfying the relation

$$N_+(\cos \alpha_{sw}) = 0, \qquad y > 0, \qquad (39)$$

$$N_+(\kappa \cos \alpha_{tsw}) = 0, \qquad y < 0, \qquad (40)$$

and the branch point singularities located at $\alpha_t = \alpha_{tb}^{\pm}$ are implicit in $M_-(\kappa \cos \alpha_t)$ and $N_-(\kappa \cos \alpha_t)$. Neglecting the branch cut contribution, we find that a uniform expression for the scattered field is given by

$$E_z^s = \sqrt{\frac{2\pi}{k\rho}} P^e(\cos \phi) e^{-jk\rho} e^{j\pi/4}$$

$$+ \frac{1}{2}\sqrt{\frac{2\pi}{k\rho}} \frac{t_1^e(\alpha_{go}^-, \phi_0)}{\sin \alpha_{go}^-} \sec\left(\frac{\phi - \alpha_{go}^- + \pi}{2}\right)\left\{1 - F_{kp}\left[2k\rho \cos^2\left(\frac{\phi - \alpha_{go}^- + \pi}{2}\right)\right]\right\} e^{-jk\rho} e^{j\pi/4}$$

$$+ \frac{1}{2}\sqrt{\frac{2\pi}{k\rho}} \frac{t_1^e(\alpha_{go}^+, \phi_0)}{\sin \alpha_{go}^+} \sec\left(\frac{\phi - \alpha_{go}^+ - \pi}{2}\right)\left\{1 - F_{kp}\left[2k\rho \cos^2\left(\frac{\phi - \alpha_{go}^+ - \pi}{2}\right)\right]\right\} e^{-jk\rho} e^{j\pi/4} \qquad (41)$$

$$- \frac{1}{2}\sqrt{\frac{2\pi}{k\rho}} \frac{t_2^e(\alpha_{sw}, \phi_0)}{N'(\cos \alpha_{sw})} \sec\left(\frac{\phi - \alpha_{sw} + \pi}{2}\right)\left\{1 - F_{kp}\left[2k\rho \cos^2\left(\frac{\phi - \alpha_{sw} + \pi}{2}\right)\right]\right\} e^{-jk\rho} e^{j\pi/4}$$

for $y > 0$ and

$$E_z^{st} = \kappa\left\{\sqrt{\frac{2\pi}{\kappa k\rho}} Q(\kappa \cos \phi) e^{-j\kappa k\rho} e^{j\pi/4}\right.$$

$$+ \frac{1}{2}\sqrt{\frac{2\pi}{\kappa k\rho}} \frac{t_{1t}^e(\alpha_{tgo}^-, \phi_0)}{\kappa \sin \alpha_{tgo}^-} \sec\left(\frac{\phi + \alpha_{tgo}^- - \pi}{2}\right)\left\{1 - F_{kp}\left[2\kappa k\rho \cos^2\left(\frac{\phi + \alpha_{tgo}^- - \pi}{2}\right)\right]\right\} e^{-j\kappa k\rho} e^{j\pi/4}$$

$$+ \frac{1}{2}\sqrt{\frac{2\pi}{\kappa k\rho}} \frac{t_{1t}^e(\alpha_{tgo}^+, \phi_0)}{\kappa \sin \alpha_{tgo}^+} \sec\left(\frac{\phi + \alpha_{tgo}^+ + \pi}{2}\right)\left\{1 - F_{kp}\left[2\kappa k\rho \cos^2\left(\frac{\phi + \alpha_{tgo}^+ + \pi}{2}\right)\right]\right\} e^{-j\kappa k\rho} e^{j\pi/4}$$

$$\left. - \frac{1}{2}\sqrt{\frac{2\pi}{\kappa k\rho}} \frac{t_{2t}^e(\alpha_{tsw}, \phi_0)}{N'(\kappa \cos \alpha_{tsw})} \sec\left(\frac{\phi + \alpha_{tsw} + \pi}{2}\right)\left\{1 - F_{kp}\left[2\kappa k\rho \cos^2\left(\frac{\phi + \alpha_{tsw} + \pi}{2}\right)\right]\right\} e^{-j\kappa k\rho} e^{j\pi/4}\right\} \qquad (42)$$

for $y < 0$. In the above

$$t_1^e(\alpha, \phi_0) = P^e(\cos \alpha)(\cos \phi_0 + \cos \alpha), \tag{43}$$

$$t_{1t}^e(\alpha_t, \phi_0) = Q(\kappa \cos \alpha_t)(\cos \phi_0 + \kappa \cos \alpha_t), \tag{44}$$

$$t_2^e(\alpha, \phi_0) = P^e(\cos \alpha) \frac{N_+(-\cos \alpha) \, N_+(\cos \alpha)}{N(\cos \alpha)}, \tag{45}$$

$$t_{2t}^e(\alpha_t, \phi_0) = Q(\kappa \cos \alpha_t) \frac{N_+(-\kappa \cos \alpha_t) \, N_+(\kappa \cos \alpha_t)}{N(\kappa \cos \alpha_t)}, \tag{46}$$

$$N'(\cos \alpha_{sw}) = \frac{R}{Z_0} \cos \alpha_{sw} \left[1 + \frac{1}{\mu_r} \frac{\sin \alpha_{sw}}{\sqrt{\kappa^2 - \cos^2 \alpha_{sw}}} \right], \tag{47}$$

$$N'(\kappa \cos \alpha_{tsw}) = \frac{R}{Z_0} \kappa \cos \alpha_{tsw} \left[\frac{\kappa \sin \alpha_{tsw}}{\sqrt{1 - \kappa^2 \cos^2 \alpha_{tsw}}} + \frac{1}{\mu_r} \right], \tag{48}$$

and the lower sign is always chosen in (28) for the computation of $F_{kp}(z)$. As before, we observe that the first terms in the expressions for the scattered fields is simply the non-uniform result. The non-uniform diffraction coefficients are thus given by

$$D^e(\phi, \phi_0) = \sqrt{\frac{2\pi}{k}} \, P^e(\cos \phi) \, e^{j\pi/4}, \qquad y > 0, \tag{49}$$

$$D_t^e(\phi, \phi_0) = \kappa \sqrt{\frac{2\pi}{\kappa k}} \, Q(\kappa \cos \phi) \, e^{j\pi/4}, \quad y < 0. \tag{50}$$

4. Computational results

In this section, several examples of the diffraction and total field patterns are presented. Two sets of dielectric parameters, along with three different values for the resistivity are considered. We note that if the resistive half sheet is to represent a dielectric step, then R is defined by [1, 2] as

$$R = \frac{-jZ_0}{(\varepsilon_r' - 1)k_0 \tau} \tag{51}$$

assuming $\mu_r' = 1$, where ε_r' and μ_r' are the relative permittivity and permeability, respectively, of the simulated layer, and τ is the thickness (height) of the layer (step). Accordingly, the value of $R/Z_0 = -j\,0.8$ may correspond to a dielectric step having $\varepsilon_r' = 3$, $\mu_r' = 1$ and $\tau = 0.1\lambda$.

Defining the echowidth σ as

$$\sigma = 2\pi |D(\phi, \phi_0)|^2,$$

Figs. 5 and 6 present E_z and H_z echowidth patterns. Each figure contains curves corresponding to the resistive half planes having $R = 0$, $-j\,0.8$, and 0.25 and in the presence of dielectric interfaces having either $\varepsilon_r = 2$, $\mu_r = 1$ or $\varepsilon_r = 5 - j\,0.5$, $\mu_r = 1.5 - j\,0.1$. When compared to the echowidth of an isolated perfectly conducting half plane, a scattering reduction is observed in all cases.

To illustrate the effect of the branch cut singularity, Fig. 7 shows the magnitude of the E_z non-uniform diffracted field (first terms of (41) and (42)) observed at $\rho = 1.6\lambda$. The slope discontinuities near $\phi = 225°$
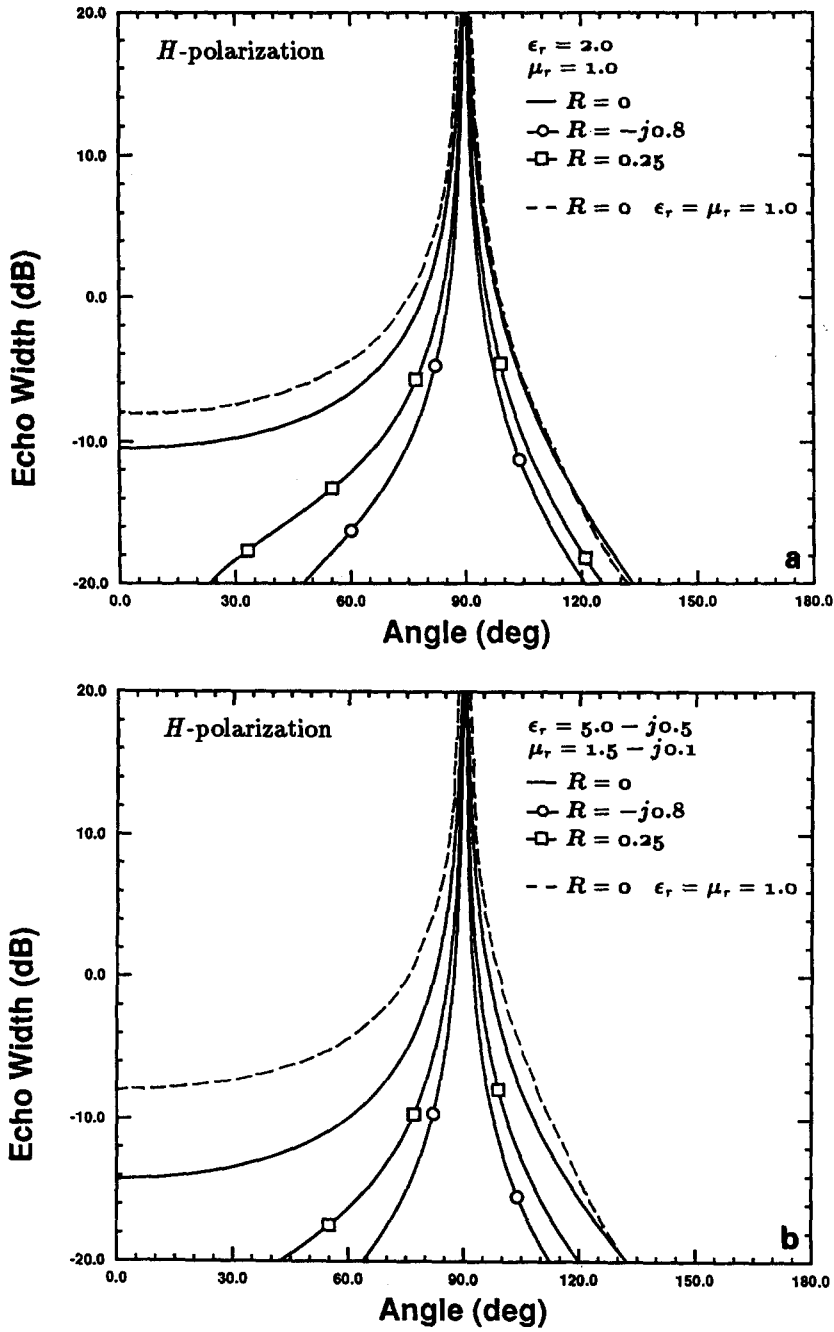
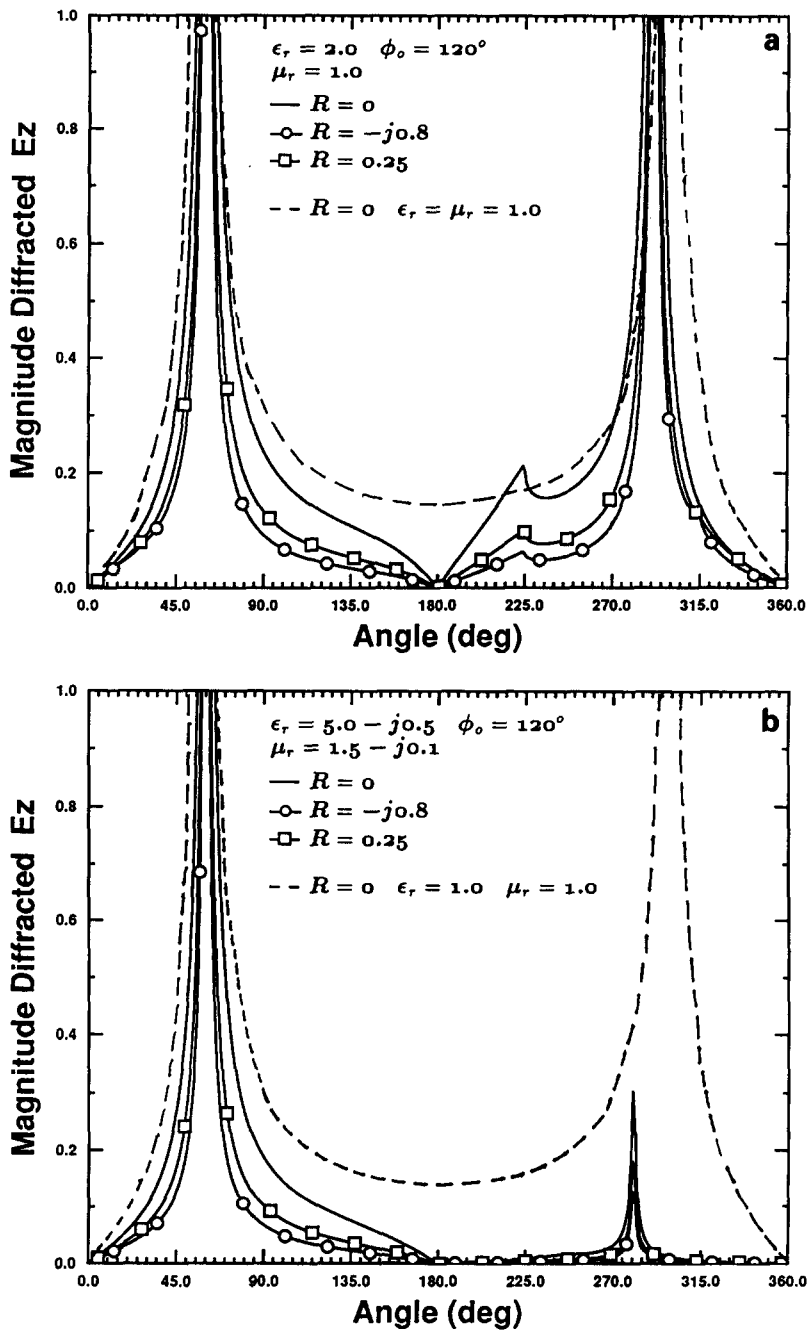Fig. 5. Backscatter diffraction patterns for H-polarization.

Fig. 6. Backscatter diffraction patterns for E-polarization.
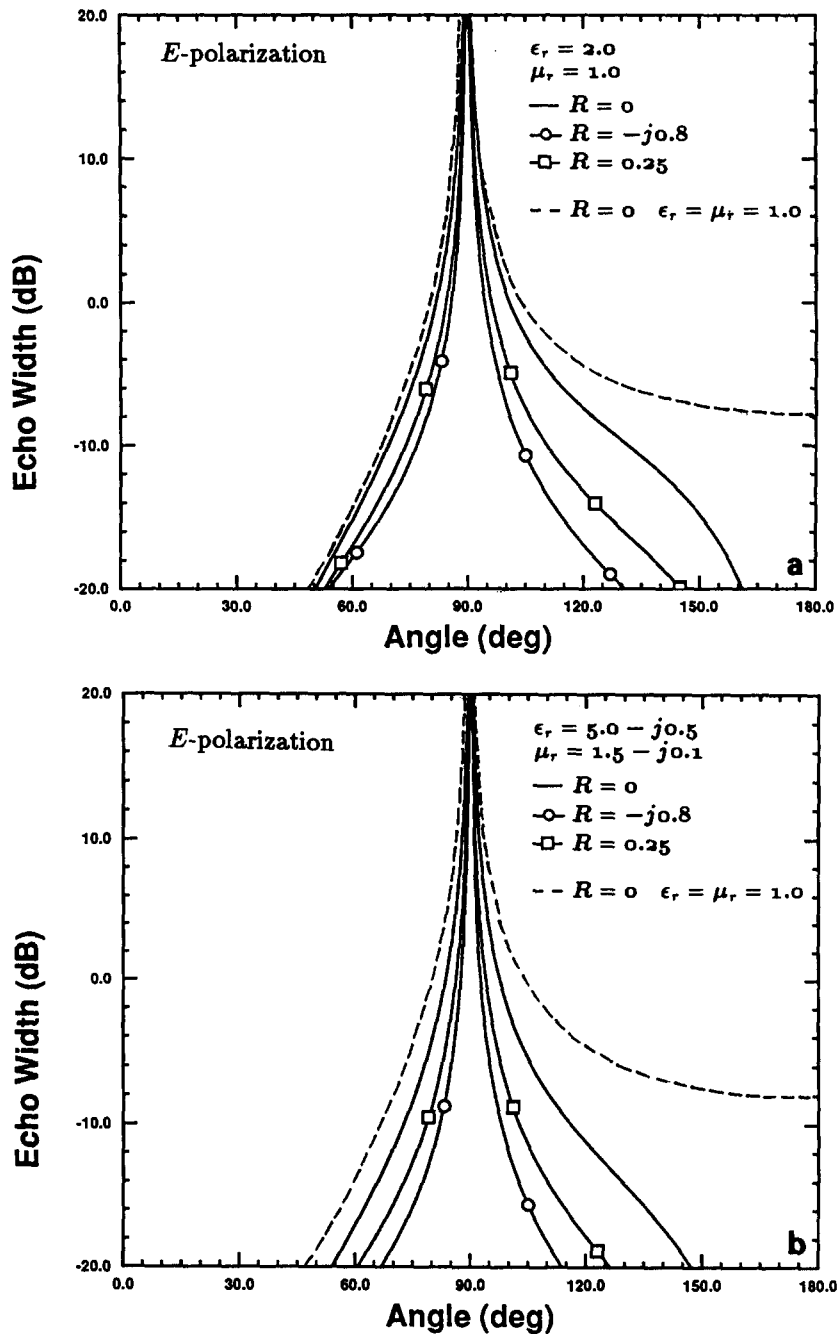
Fig. 7. Bistatic diffraction patterns for E-polarization at $\rho = 1.6\lambda$.
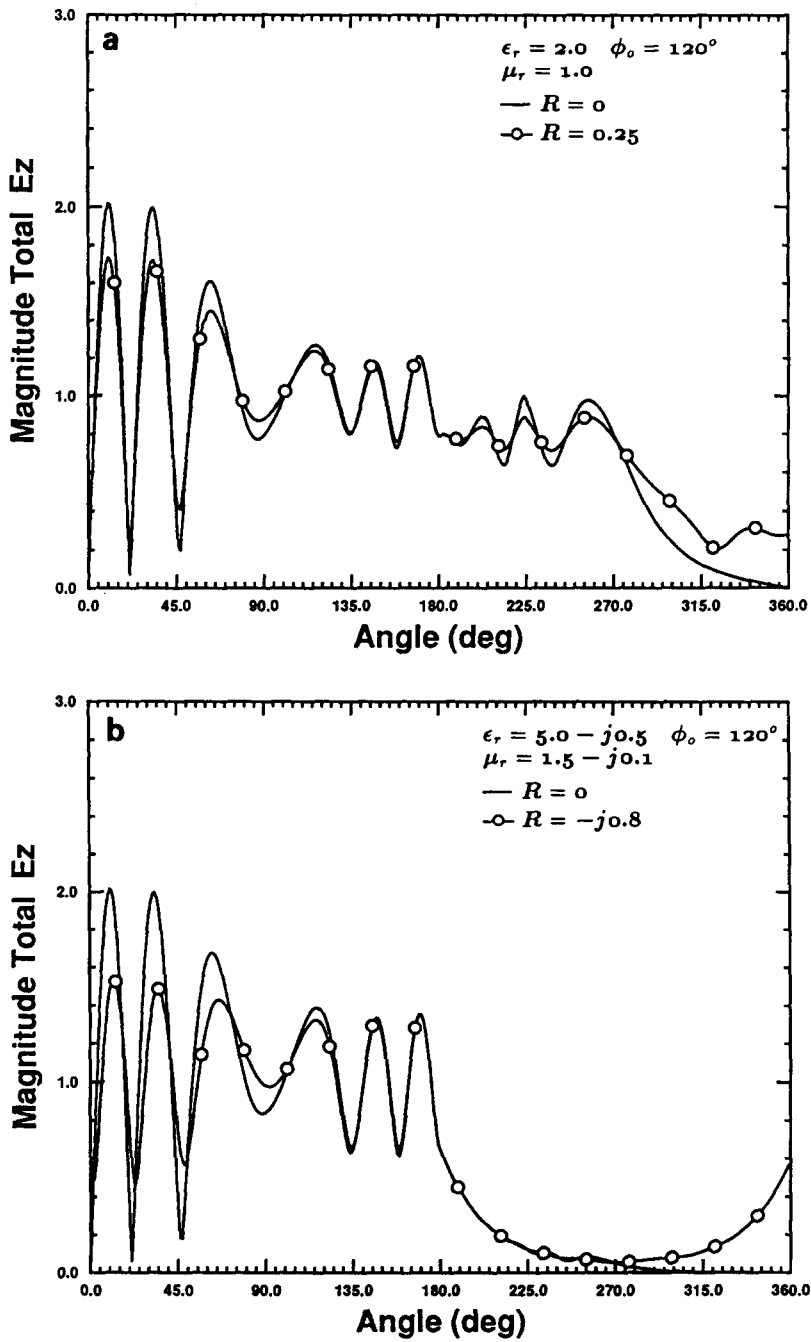
Fig. 8. Total field patterns for *E*-polarization.

in Fig. 7a are due to the function $M_-(\kappa \cos \alpha_t)$ and occur at the point where the steepest descent path crosses the branch cut. We note that this behavior has already been seen in [8] for $R = 0$. Since a branch cut is also associated with the split function $N_+(\lambda)$, a similar but less distinct slope discontinuity occurs near $\phi = 315°$, where the appropriate branch cut is crossed. Referring to the patterns in Fig. 7b, the losses in the dielectric region are quite significant yielding nearly zero diffracted field in that region. In Fig. 8, the total field patterns given by (41) and (42) are shown for $\rho = 1.6\lambda$. The slope discontinuity at $\phi = 225°$ in still seen in Fig. 8a. However, the one near $\phi = 315°$ is not visible. A similar slope discontinuity in the total field is also observed at $\phi = 180°$ for all patterns, and this is clearly due to the rapidly varying nature of the diffracted field as can be ascertained from an examination of the patterns in Fig. 7. It is expected that all of the above slope discontinuities would disappear upon performing a uniform evaluation of the branch cut contribution.

5. Summary

The problem of diffraction by a resistive half sheet on a dielectric interface was treated via the angular spectrum method, otherwise referred to as the dual integral equation approach. Both E- and H-polarizations were considered. The solution required the introduction of the two Wiener-Hopf split functions, one generic to the dielectric interface and another characteristic to the presence of the resistive half plane. For their evaluation we resorted to a convenient numerical procedure given in the Appendix.

A uniform asymptotic evaluation was performed for the resulting scattered field integral accounting for the presence of the geometrical optics and surface wave poles. Unfortunately, a uniform evaluation of the branch point singularity was not possible using traditional techniques. Because of this, a slight slope discontinuity was observed in the computed near zone total field patterns.

Acknowledgment

The authors wish to thank Mark A. Ricoy for helpful comments and suggestions.

Appendix

The factorization of G, J, M, and N herein is accomplished by using a recently derived integral expression [7]. If $F(\lambda)$ denotes the function to be factorized such that $F(\lambda)$ is regular in the strip $\tau^- < \text{Im}(\lambda) < \tau^+$ ($\tau^\pm$ can generally be arbitrarily small) and $F(\lambda) \to 1$ uniformly as $|\lambda| \to \infty$, then $F(\lambda)$ can be factorized as [14]

$$F(\lambda) = U(\lambda) L(\lambda) \tag{A.1}$$

where $U(\lambda)$ is regular in the region $\text{Im}(\lambda) > \tau^-$, and $L(\lambda)$ is regular in the region $\text{Im}(\lambda) < \tau^+$. From [7],

$$U(\lambda) = L(-\lambda) = e^{H(\lambda)}, \quad \text{Im}(\lambda) > 0 \tag{A.2}$$

where

$$H(\lambda) = \tfrac{1}{2}\ln[F(\lambda)] + \frac{\lambda \, e^{j\theta}}{2j} \int_0^1 \frac{\ln[F\{e^{j\theta} \tan \pi\nu/2\}] - \ln[F(\lambda)]}{\sin^2 \pi\nu/2 \, e^{j2\theta} - \lambda^2 \cos^2 \pi\nu/2} \, d\nu \tag{A.3}$$

in which $0 < \theta < \frac{1}{2}\pi$, and should be chosen such that $F(\nu)$ exhibits a rapid decay as ν increases from 0 to 1. We note that (A.3) was derived from the formal factorization expression given in [14] and is therefore exact.

References

[1] T.B.A. Senior, "Combined resistive and conductive sheets", *IEEE Trans. Antennas Propagat 33*, 577–579 (1985).

[2] M.I. Herman and J.L. Volakis, "High frequency scattering by a resistive strip and extensions to conductive and impedance strips", *Radio Sci. 22*, 335–349 (1987).

[3] H.G. Booker and P.C. Clemmow, "The concept of an angular spectrum of plane waves and its relation to that of polar diagrams and aperture distributions", *Proc. Inst. Elect. Eng. 97*, 11–17 (1950).

[4] P.C. Clemmow, "A method for the exact solution of a class of two dimensional diffraction problems", *Proc. Roy. Soc. A. 205*, 286–308 (1951).

[5] J.L. Volakis and M.A. Ricoy, "Diffraction by a thick perfectly conducting half-plane", *IEEE Trans. Antennas Propagat. 35*, 62–72 (1987).

[6] J.L. Volakis, "Scattering by a thick impedance half plane", *Radio Sci. 22*, 13–25 (1987).

[7] M.A. Ricoy and J.L. Volakis, "*E*-polarization diffraction by a thick metal-dielectric join", *J. Electromagnetic Waves Appl. 3* (5), 383–407 (1989).

[8] R.D. Coblin and L.W. Pearson, "A geometrical theory of diffraction for a half plane residing on the interface between dissimilar media: Transverse magnetic polarization case", *Radio Sci. 19*, 1277–1288 (1984).

[9] P.C. Clemmow, "Radio propagation over a flat earth across a boundary separating two different media", *Proc. Roy. Soc. A 246*, 1–55 (1953).

[10] T.B.A. Senior, "Diffraction by a semi-infinite metallic sheet", *Proc. Roy. Soc. A 213*, 436–458 (1952).

[11] J.L. Volakis and M.I. Herman, "A uniform asymptotic evaluation of integrals", *Proc. IEEE 74*, 1043–1044 (1986).

[12] R.G. Kouyoumjian and P.H. Pathak, "A uniform geometrical theory of diffraction for an edge in a perfectly conducting surface", *Proc. IEEE 62*, 1447–1461 (1974).

[13] R.H. Schafer and R.G. Kouyoumjian, "Higher order terms in the saddle point approximation", *Proc. IEEE 55*, 1496–1497 (1967).

[14] B. Noble, *Methods Based on the Wiener–Hopf Technique*, Pergamon Press, Oxford (1958).